ID: 713

Spatially Dependent Simulations and Model Validation of Runaway Electron Dissipation Via Impurity Injection In DIII-D and JET Using KORC

***M.T. Beidler*[1]**, D. Del-Castillo-Negrete[1], L.R. Baylor[1], J.L. Herfindal[1], D. Shiraki[1], D.A. Spong[1], E.M. Hollmann[2], M. Lehnen[3], C. Reux[4], and JET Contributors[5]

[1]Oak Ridge National Laboratory; [2]University of California-San Diego; [3]ITER Organization; [4]CEA, IRFM; [5]EUROfusion Consortium

beidlermt@ornl.gov

ABSTRACT

- The Kinetic Orbit Runaway electrons Code (KORC) is extended to model post-disruption runaway electron (RE) mitigation by secondary impurity injection.
- KORC simulations indicate that RE beam evolution is a delicate balance between collisional and drift orbit effects in an evolving magnetic configuration.
- Inclusion of neutral impurity transport in collision operators has a significant effect on RE ensemble evolution and is required for agreement with experiments.

INTRODUCTION

- Because ITER is designed with water-cooled, plasma-facing components (PFCs) with cooling tubes near the plasma-facing surface, REs pose a severe risk for water leaks.
- Disruption and RE mitigation systems using shattered pellet injection (SPI) or massive gas injection (MGI) must be extrapolated from existing devices to ITER.
- KORC [1] has been extended [2] to use time-sequenced, experimental, magnetic reconstructions, a spatiotemporal (ST) density model fit to experimental line integrated density (LID) measurements, and collision operators including partially-ionized impurities [3].
- This work uses KORC to model impurity injection into post-disruption RE beams in DIII-D discharge #164409 with Ne MGI and JET pulse #95128 with Ar SPI.

KORC PHYSICS MODEL

TIME-SEQUENCED EXPERIMENTAL, MAGNETIC RECONSTRUCTIONS

Guiding center (GC) equations in cylindrical coordinates (R, ϕ, Z) and synchrotron radiation are evaluated using magnetic and electric fields from experimental reconstructions. JFIT and EFIT reconstructions are used for DIII-D and JET, respectively, with poloidal field $\boldsymbol{B}_p = 1/2\pi\, \nabla\phi \times \nabla\psi_p$, toroidal field $B_\phi = R_0 B_0 / R$, and inductive toroidal electric field $\mathrm{E}_\phi = -1/2\pi R\, \partial\psi_p/\partial t$. Examples of instantaneous poloidal flux contours of DIII-D and JET are shown in Fig. 1.

SPATIOTEMPORAL DENSITY MODEL

A Fokker-Planck linearized Coulomb collision operator and bremsstrahlung radiation are evaluated using an ST density model fit to experimental LID measurements. The ST density model (dashed) and comparison to the LID (solid) is shown in Fig. 1., and all partially-ionized impurities are modeled to have the same profile as electrons. Only lower ionization states are included due to the $\leq 2\mathrm{eV}$ temperature of thermal plasma. A uniform neutral impurity profile is also included. Large angle collisions, comprising an "avalanche" RE source, are not included. However, calculation of the avalanche growth rate for JET indicates large angle collisions are required for accurate modeling and a large angle collision operator is presently being implemented in KORC.

RE BEAM INITIALIZATION

Simulations use a monoenergy/pitch RE beam with $10\ \mathrm{MeV}/10°$ (unless otherwise noted). REs are initialized spatially uniform within $\psi_N = 0.845$ to be confined within each configuration.

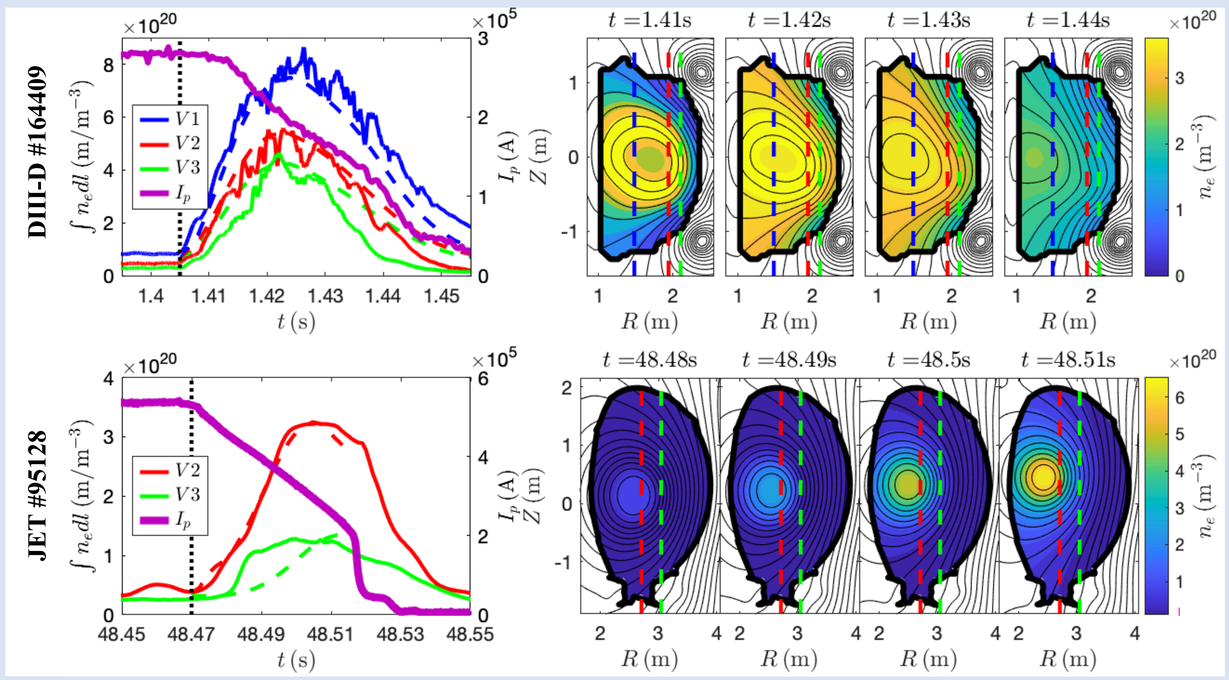

FIG. 1. Snapshots of magnetic configuration and density model used in KORC calculations

RESULTS

RE MITIGATION SIMULATIONS

Figure 2. shows KORC simulations of RE mitigation where the RE energy and current is given by

$$\mathcal{E}_{\mathrm{RE}} = m_e c^2 \sum_i^{N_{\mathrm{RE}}} \gamma_i\, \mathcal{H}_{\mathrm{RE},i}, I_{\mathrm{RE}} = -\frac{e}{2\pi} \sum_i^{N_{\mathrm{RE}}} \frac{v_\phi}{R_i} \mathcal{H}_{\mathrm{RE},i}, \text{where } \mathcal{H}_{\mathrm{RE},i} = \begin{cases} 1 & \text{if } p_i > m_e c \\ 0 & \text{if } p_i < m_e c \text{ or hits wall.} \end{cases}$$

The modeled RE current agrees well throughout the RE mitigation phase for DIII-D, while there is less agreement in the latter part of the JET simulation. We posit that the lack of an avalanche RE source and uncertainty in the neutral impurity transport, and in general, the plasma and partially-ionized impurity transport, is causing the disparity. Another calculation using a simplified hollow neutral profile, in line with expectations from Ref. [4], yields better agreement with experiment (not shown). Improved neutral transport modeling will be addressed in future work by coupling KORC to the 1D plasma and impurity transport model in Ref. [4]. Due to the improved confinement and increased collisionality

RE ENERGY DEPOSITION

The wall deposition pattern on the inner wall limiter is assumed axisymmetric and is qualitatively different in the two cases. DIII-D has the RE beam advect toward the wall due to less effective horizontal position control at low current, while JET advects inward toward and upward along the wall while beginning a vertical displacement event. This upward advection increases the total area over which REs deposit their energy and may prove beneficial. The maximum total power deposited on the inner wall is approximately a factor of 5 larger for JET than DIII-D (not shown).

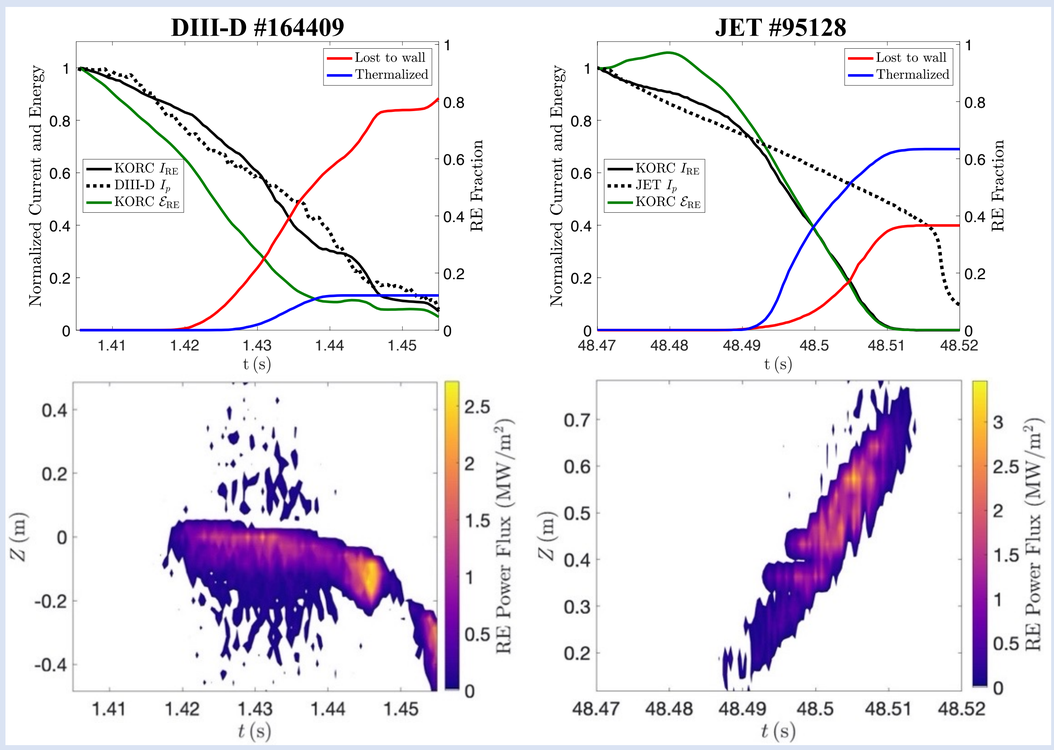

FIG. 2. KORC simulations of RE mitigation in DIII-D #164409 and JET #95128

IMPORTANCE OF SPATIAL EFFECTS

Drift orbits of fixed-energy passing particles in an axisymmetric, circular cross-section, magnetic configuration with a constant safety factor q_0 can be approximated by by shifted circles

$$(R-\Delta)^2 + Z^2 = R_c^2, \text{with } \Delta = R_0 + \frac{q_0 v_\phi}{\Omega_e} \text{ and } R_c^2 = \Delta^2 - R_0^2 + \frac{2 q_0 v_\phi}{\Omega_e},$$

where $\Omega_e = eB/\gamma m_e$ is the relativistic gyrofrequency, and $v_\phi \simeq v\cos\eta$ with pitch angle η. Collisions reduce the drift orbit effects through slowing down and pitch angle scattering, however, pitch angle scattering also decreases the current, increasing q_0. Figure 3 shows the effect of including neutral impurities on drift orbits, where REs are lost to the high/low field side (HFS/LFS) with/without neutrals. The balance between collisional effects and drift orbit effects in an evolving magnetic configuration is further illustrated by the parametric scan of RE energy in Fig. 4. As energy increases, drift orbit effects decrease the confinement region yielding immediate losses and lead to spatial redistribution from the HFS to LFS of the gradual deconfinement. More details can be found in Ref. [5].

FIG. 3. Effect of neutral impurities on balance of drift orbit and collisional effects in DIII-D

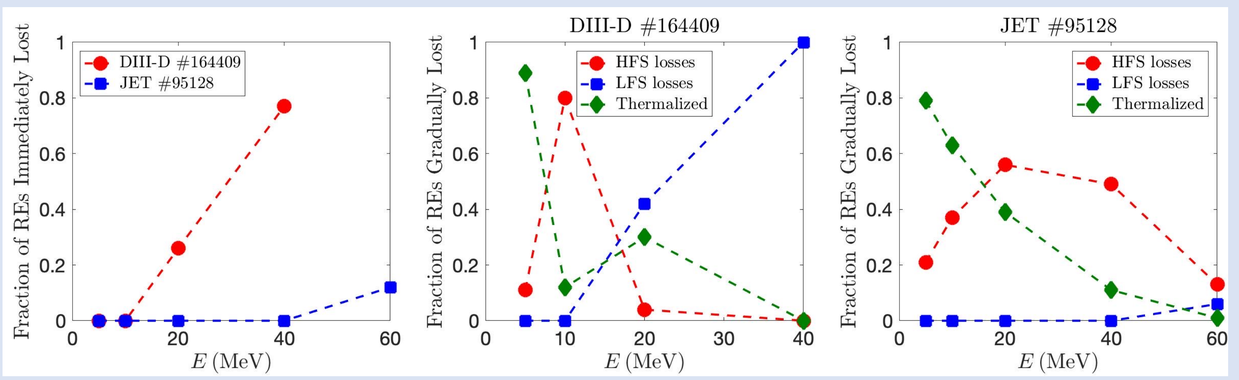

FIG. 4. Parametric scan of RE energy and effects on confinement and thermalization

CONCLUSIONS

- KORC simulations of RE mitigation show a delicate balance between collisional effects including partially-ionized impurities and drift orbit effects in an evolving magnetic configuration.
- Inclusion of neutral impurity transport in collision operators has a significant effect on RE ensemble evolution and is required for agreement with experiments.
- Inclusion of avalanche RE source and accurate modeling of plasma and impurity transport, including neutrals, is required, and coupling to 1D transport model from Ref. [4] is underway.

ACKNOWLEDGEMENTS / REFERENCES

- The authors thank C. Maggi and D. Terranova for providing EFIT reconstructions of JET pulse #95128.
- This work was supported by the US DOE under contracts DE-AC05-00OR22725 and DE-FC02-04ER54698 and by the ITER Organization (TA C18TD38FU) and carried out within the framework of the EUROfusion Consortium, receiving funding from the Euratom research and training programme 2014-2018 and 2019-2020 under grant agreement No 633053. The views and opinions expressed herein do not necessarily reflect those of the European Commission or the ITER Organization. This research used resources of the National Energy Research Scientific Computing Center (NERSC), a U.S. Department of Energy Office of Science User Facility operated under Contract No. DE-AC02-05CH11231.

[1] Carbajal et al., Phys. Plasmas **25** (2017) 042512. [2] Beidler et al., Phys. Plasmas **27** (2020) 112507.
[3] Hesslow et al., Phys. Rev. Lett. **118** (2017) 255001. [4] Hollmann et al., Nucl. Fusion **59** (2019) 106014.
[5] del-Castillo-Negrete et al., IAEA FEC 2020, Poster 1011.